View metadata, citation and similar papers at core.ac.uk
brought to you by CORE
provided by Italian Group Fracture (IGF): E-Journals / Gruppo Italiano Frattura

M. Vormwald et alii, Frattura ed Integrità Strutturale, 41 (2017) 314-322; DOI: 10.3221/IGF-ESIS.41.42

Focused on Crack Tip Fields

# Variable mode-mixity during fatigue cycles – crack tip parameters determined from displacement fields measured by digital image correlation

Michael Vormwald, Yigiter Hos
*Technische Universität Darmstadt, Materials Mechanics Group, Franziska-Braun-Str. 3, D-64287 Darmstadt, Germany*
*vormwald@wm.tu-darmstadt.de, hos@wm.tu-darmstadt.de*

José L.F. Freire, Giancarlo L.G. Gonzáles, Jorge G. Díaz
*Pontifícia Universidade Católica do Rio de Janeiro, PUC-Rio, Rua Marquês de São Vicente, 225, Gávea - Rio de Janeiro, Brasil*
*jlfreire@puc-rio.br, gonzalesglg@aaa.puc-rio.br, jorgegdiaz@aluno.puc-rio.br*

**ABSTRACT.** This paper focusses on discussing equivalent stress intensity factors and kink angles after a change of mode-mixity from one cycle to the next and when the mode-mixity changes continuously during the fatigue cycles. Thin-walled tubes with through-wall cracks have been loaded by proportional and non-proportional tension and torsion. In the experimental investigation, the region of fatigue crack growth was observed by applying the digital image correlation technique. Data on the variations of the displacement and strain fields during the cycles were acquired and used to determine mixed-mode variations of stress intensity factors associated with opening modes I, II and III. For each specific specimen the crack path was observed in order to relate its curvature – both kinks and continuously developing warped cracks – with the variations of the displacement field and associated stress intensity factors.

**KEYWORDS.** Mixed-mode; Fatigue crack growth; Digital image correlation; Crack kinking.

OPEN ACCESS

**Citation:** Vormwald, M., Hos, Y., Freire, J. L. F., Gonzáles, G.L.G., Díaz J. G., Variable mode-mixity during fatigue cycles – crack tip parameters determined from displacement fields measured by digital image correlation, Frattura ed Integrità Strutturale, 41 (2017) 314-322.

**Received:** 28.02.2017
**Accepted:** 03.05.2017
**Published:** 01.07.2017

**Copyright:** © 2017 This is an open access article under the terms of the CC-BY 4.0, which permits unrestricted use, distribution, and reproduction in any medium, provided the original author and source are credited.

## INTRODUCTION

Thorough reviews on crack-path evolution rules and on fatigue crack-growth under non-proportional mixed-mode loading were presented by Mróz et al. [1] and Zerres et al. [2]. Schöllmann et al. [3], Richard and co-workers [4-6] and Yang et al. [7] presented, discussed criteria for the prediction of crack growth, and summarized findings for 2D and 3D components subjected to multiaxial loading. Analysis of the literature review revealed that it is still an open question the determination of equivalent stress intensity factors, SIF, as well as crack growth rules and the prediction of crack path tangent for complex opening-mode problems, mainly if opening mode III is present. The influence of several variables such as: structural component geometry and material, load mode-mixity, presence of all three opening modes, nominal load range ratio R, local crack tip effects including plasticity and 3D corner effects [8], crack flank roughness, crack closure and crack blunting, make the understanding of the fatigue crack growth an extraordinary problem. A

generally accepted and validated formulation of a crack force parameter still needs to be identified [2]. Moreover, experimental investigations for the 3D mixed mode load to validate existing predicting assumptions need to be further developed [4]. The present paper discusses 2D and 3D formulations for equivalent SIFs for complex mode problems, presented by Erdogan and Sih [9], by Schöllmann et al. [3] and by Richard et al. [4-6], under the light of experiments carried out by Vormwald and his co-workers [10, 11]. These experiments used digital image correlation, DIC, to measure full-field displacement and derived data for 3D tested specimens. The acquired data made possible the determination of relative crack flank opening displacements, COD, and their associated mode I, II and III SIFs, as well as the calculation of equivalent SIFs and tangents to crack paths for cases of mixed-mode variations (inside one cycle and from cycle to cycle) using the above mentioned formulations.

## EXPERIMENTAL METHODS

Constant amplitude fatigue tests have been performed using thin-walled tubes under alternated tension-compression (force $F$ ranging from 45kN to -45kN) and torsion (moment $M$ ranging from 532 Nm to -532 Nm). Data was acquired from five different loading sequences applied to individual specimens [2-3]: pure alternated tension-compression loading (specimen R-028), pure alternated torsion loading (specimen R-029), proportional alternated tension and torsion loading (specimen R-030), and out-of-phase loading with phase angles of 45° (specimen R-033) and 90° (specimen R-031). The load ratio was $R_F = R_M = -1$. The specimen geometry is shown in Fig. 1. The specimens were machined from longitudinally welded tubes. The individual specimens were saw-cut and the slits or notches were milled. Two holes, with a diameter of 4 mm, were drilled with a distance of 10 mm from the centers of the holes (length of an arc measured at the outer surface). The notch was positioned opposite to the longitudinal weld. The material was constructional steel S235 with the following mechanical properties: Young's modulus, $E$ = 214GPa, yield strength (0.2% plastic offset), $S_y$ = 310MPa, ultimate tensile strength $S_u$ = 435MPa, and the parameters of the cyclic Ramberg-Osgood stress-strain curve, $K'$ and $n'$, respectively equal to 1170MPa and 0.239.

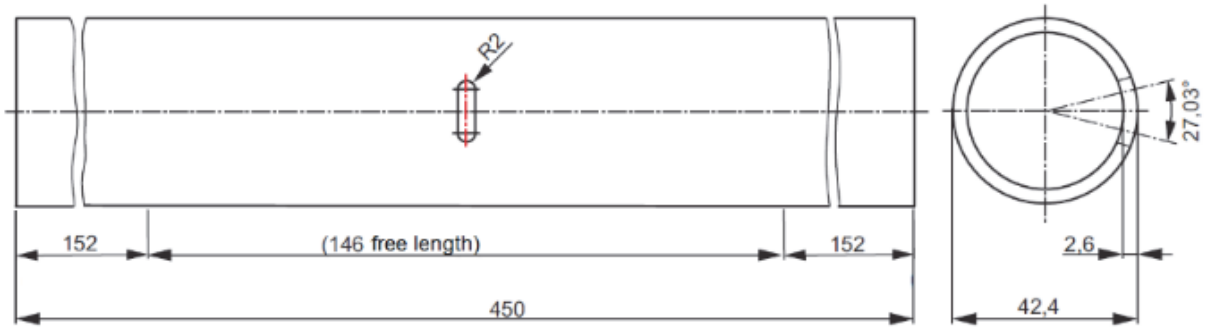


Figure 1: Specimen geometry (mm)

The experiments have been conducted under load and moment control, respectively, using a servo-hydraulic, four-pillar tension-torsion testing machine with frequencies between 0.1 Hz (when necessary, during 3 cycles for DIC data acquisition) and 2 Hz. The cracks were assumed to be through-wall cracks with a straight crack front. The crack length is defined as the arc length with the arc measured starting at the crack initiation location. Depending on the loading type, two, or four cracks were observed [10, 11].

## DETERMINATION OF STRESS INTENSITY FACTORS FROM CRACK-FLANK OPENING DISPLACEMENTS

The determination of SIFs, $K_i$ (i = I, II, III) was based on their relationship with relative crack flank opening displacements, $COD_i$, [12] as given by Eqs. (1). Generally, points A and B are symmetrically located over the crack faces ($\theta \sim \pm\pi$) and near the crack tip (small local crack path curvature and coordinate r << crack length a), as illustrated in Fig. 2. In Eq. (1) U', V' are in plane displacements respectively in the parallel and orthogonal crack directions and W' is the out of plane displacement. Polar coordinates are referred to the tangent and orthogonal axes relative to the crack line.

$$K_I = \frac{E(COD_I)}{2(1+\nu)}\left[\sqrt{\frac{r_A}{2\pi}}\sin(\frac{\theta_A}{2}).\left(\frac{2}{1+\nu}-\cos^2(\frac{\theta_A}{2})\right)-\sqrt{\frac{r_B}{2\pi}}\sin(\frac{\theta_B}{2}).\left(\frac{2}{1+\nu}-\cos^2(\frac{\theta_B}{2})\right)\right]^{-1}$$

$$K_{II} = \frac{E(COD_{II})}{2(1+\nu)}\left[\sqrt{\frac{r_A}{2\pi}}\sin(\frac{\theta_A}{2}).\left(\frac{2}{1+\nu}+\cos^2(\frac{\theta_A}{2})\right)-\sqrt{\frac{r_B}{2\pi}}\sin(\frac{\theta_B}{2}).\left(\frac{2}{1+\nu}+\cos^2(\frac{\theta_B}{2})\right)\right]^{-1} \quad (1)$$

$$K_{III} = \frac{E(COD_{III})}{4(1+\nu)}\left[\sqrt{\frac{r_A}{2\pi}}\sin(\frac{\theta_A}{2})-\sqrt{\frac{r_B}{2\pi}}\sin(\frac{\theta_B}{2})\right]^{-1}$$

$$COD_I = V'_A - V'_B \quad COD_{II} = U'_A - U'_B \quad COD_{III} = W'_A - W'_B$$

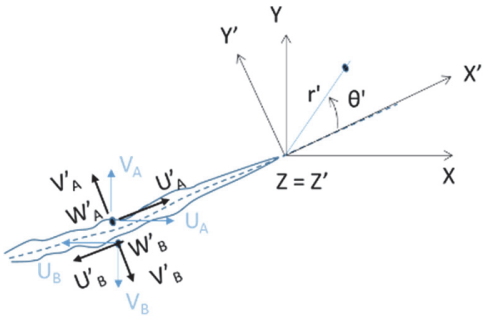


Figure 2: Displacements at points A, B located on the crack-flank and near to the crack tip.

One advantage of using the SIF related COD formulation is the possibility of determining elastic equivalent SIFs when crack plasticity and blunting affect near field displacement or strain measurements occurring at points very close to and in front of the crack-tip. CODs are lesser influenced by particular point measurements, once they correspond to integrated displacement values of points located over the crack flanks between the measuring point (A or B) and the crack tip. The total COD measurement in such cases corresponds to an elastic component $COD_e$ plus a plastic component $COD_p$ resulting in a total SIF* or K*, [13]. The K* value therefore results from an elastic $SIF_e$ or $K_e$ plus a plastic equivalent $SIF_p$ or $K_p$. Of course, any relation between the total K* value with near crack tip stress or strain values must be understood as an equivalent linear crack tip elastic stress or strain value.

## CALCULATION OF EQUIVALENT SIFS USING DIC

For a number of 2D or 3D cracked body problems, the prediction of monotonic static fracture or the prediction of crack growth by the equivalent or comparison static stress intensity factor, $K_v$, or by the equivalent fatigue crack growth SIF range, $\Delta K_v$, can be made by a number of different formulations, as for example those proposed by references [1-6, 9]. The present paper addresses $\Delta K_v$ calculations using $K_v$ equations initially developed by Erdogan and Sih [9] for opening modes I and II and by Schöllmann et al. [3] for opening modes I, II and III and the Richard et al. [4-6] concept that SIF ranges $\Delta K_i$ can be used in place of $K_i$ to determine equivalent ranges $\Delta K_v$ in fatigue crack growth evaluations, as given by Eqs. (2) and (3).

$$\Delta K_{vES} = \cos\frac{\theta_0}{2}\left[\Delta K_I \cos^2\frac{\theta_0}{2} - \frac{3}{2}\Delta K_{II}\sin\theta_0\right] \quad (2)$$

$$\Delta K_{vS3D} = \frac{1}{2}\cos\frac{\theta_0}{2}\left[\Delta K_I \cos^2\frac{\theta_0}{2} - \frac{3}{2}\Delta K_{II}\sin\theta_0 + \sqrt{\left(\Delta K_I \cos^2\frac{\theta_0}{2} - \frac{3}{2}\Delta K_{II}\sin\theta_0\right)^2 + 4\Delta K_{III}^2}\right] \quad (3)$$

The use of Eqs. (2) and (3) is valid if the mixed-mode ratios do not change inside a specific loading cycle. When SIF ratios change inside one cycle, the $\theta_0$ angle also changes during the cycle. Therefore, it is needed to find a maximum range value

$\Delta K_{vmax}$ that would occur during one cycle by searching which angle $\theta_0$, function of the instantaneous $K_i$ occurring during the cycle, would lead to the maximum $\Delta K_v = \Delta K_{vmax}$. First, Eqs. (1) for mode I, II and III SIFs were calculated for each pair of frames (captured images) of three data acquisition cycles (300 pairs of frames). The interval between blocks of the three cycle acquired data lasted a number of cycles (500 or 1000). For example, SIFs I, II and III calculated for specimen R-031 (subjected to non-proportional (90°) out-of-phase alternated axial-torsional load) are presented in Fig. 3. The plot shows that SIF are out-of-phase. If SIFs were in phase, Eqs. (2) and (3) could be applied straightforward using the $\Delta K_{imax}$ ranges occurring in the cycle. For the out-of-phase plot of Fig. 3, the calculation of the equivalent range for the cycle using, for example, the Schöllmann et al. Eq. (3), $\Delta K_{vS3D}$, follows the herein outlined procedure. Terms $P_j$ and $Q_j$ are defined in Eq. (4) to simplify the representation of Eq. (3). The subscript j denotes each data acquisition instant inside one cycle, for example j = 1,2, …, 100 (corresponding to one full cycle) designating each triple of SIFs I, II and III to be determined along the cycle using Eqs. (1). In Eq. (4), the angle $\theta_k$ takes values from -60° to +60° in2° steps in order to find the maximum $\Delta K_{vS3Dj}$. For the pair ($P_j$, $Q_j$), depicted in the plot of Fig. 4, the square root of Eq. (4) is given by the vector $PQ_j$, while for the pair ($P_{j+n}$, $Q_{j+n}$) is given by the vector $PQ_{j+n}$. Subtraction of these vectors gives the vector range $\Delta PQ$ and its algebraic addition to ($P_j - P_{j+n}$) results in the equivalent range $\Delta K_{vS3Dj,j+n}$ depicted in Eq. (5). The representative equivalent range for the cycle will result for the maximum value of $\Delta K_{vS3Dj,j+n}$ found, after all values of $\theta_k$ had been investigated. After this search, not only the maximum range value is found, $\Delta K_{vS3D}$ , but also the crack-path tangent direction $\theta_k = \theta_0$ where it happens.

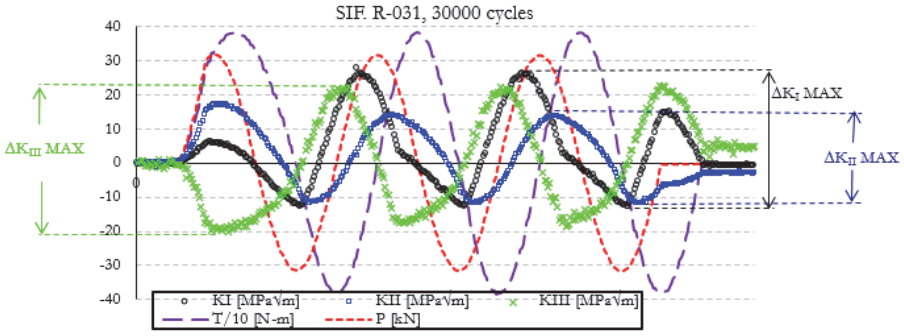


Figure 3: All mode SIF variations, ranges and applied loads as calculated from the COD method after 30,000 load cycles for a crack sizing 9.28 mm for specimen R-031 under (90°) out-of-phase alternated axial-torsional load

$$K_{vS3Dj} = P_j + \sqrt{P_j^2 + Q_j^2}$$

$$P_j = \frac{(\cos\frac{\theta_k}{2})\left(K_{Ij}\cos^2\frac{\theta_k}{2} - \frac{3}{2}K_{IIj}\sin\theta_k\right)}{2} \qquad (4)$$

$$Q_j = (\cos\frac{\theta_k}{2})\left(K_{IIIj}\right)$$

$$\Delta K_{vS3Dj,j\pm n} = \left(P_j - P_{j\pm n}\right) + \sqrt{\left(P_j - P_{j\pm n}\right)^2 + \left(Q_j - Q_{j\pm n}\right)^2} \qquad (5)$$

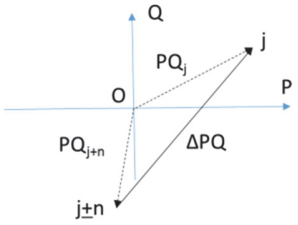


Figure 4: Calculation of the range of the square root term of Eqs. (3) and (4).

## RESULTS AND DISCUSSION

Figs. (5) to (8) present results for four of the five specimens tested. The first plot (top-left) shows the evolution of the each SIF mode and the equivalent SIF ranges with crack size. The mode I and equivalent range values are identical for specimen R-028 (single axial load), mode II and III ranges being very small. For specimens R-031 (phase angle of 90°) and R-033 (phase angle of 45°), the ratios between cycle maximum values of $\Delta K_{II}$ and $\Delta K_{I}$ change (and grow) considerably. The influence of $\Delta K_{III}$ turns out to be very important, making the equivalent 2D and 3D SIF calculated ranges differ reasonably. The second plot (bottom-left) shows the variation of the maximum I and II mode ranges with crack size. Experimentally determined crack-path tangent angle (orthogonal direction to the specimen axis) showed in the plot do not seem to be explained by the ratios between the maximum cycle values of the II and I mode SIF ranges. The third plot (top-right) shows experimentally measured ($\theta_o$) and calculated (Erdogan-Sih $\theta_o$ ES and Schöllmann et al. $\theta_o$ S3D) crack-path tangent angles for each crack length. The way the angles were calculated would impose coincidence among experimentally measured and calculated path-directions. That is seen for most cases for the determined Schöllmann et al. angles, but not seen for the Erdogan-Sih angles. The explanation comes from the fact that the 3D analyses take into consideration the large $\Delta K_{III}$ values. The forth plot (bottom-right) shows the variation of mixed-mode ratios during one cycle and from cycle to cycle. While for specimens R-028 (single axial load) and R-030 (axial and torsional proportional load) the variations are shown to be small due to reasonably proportional mixed-mode I and II ratios, the same does not happen for both out-of-phase specimens, where mode-mixity variation occurs inside each cycle and gets accentuated when the crack grows with the number of cycles.

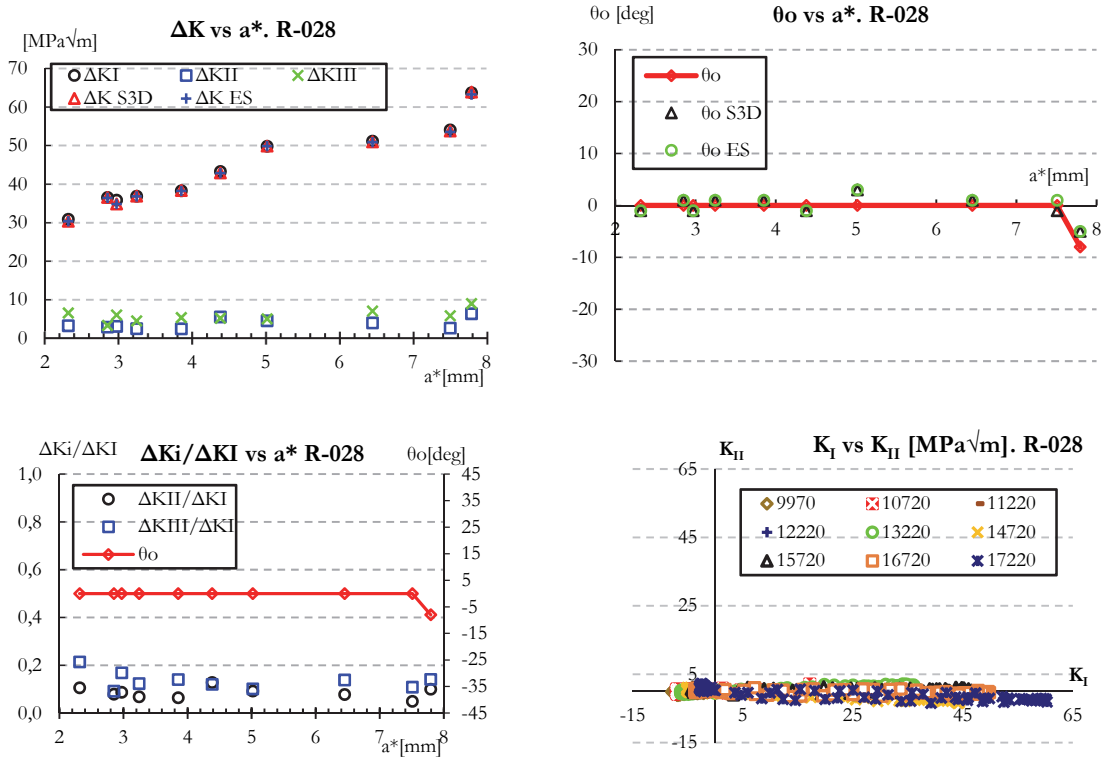


Figure 5: Crack tip parameters measured and calculated for specimen R-028, single alternated tension 45kN max. force.

## NUMERICAL INVESTIGATIONS

The first simulation is done with the specimen R-028 (single axial load). The procedure and its results have been published in ref. [14]. Summarizing, the finite-element based node-release scheme provide acceptable estimates for the effective ranges and crack growth rates could be successfully correlated with the effective cyclic $\Delta J_{eff}$-integral.

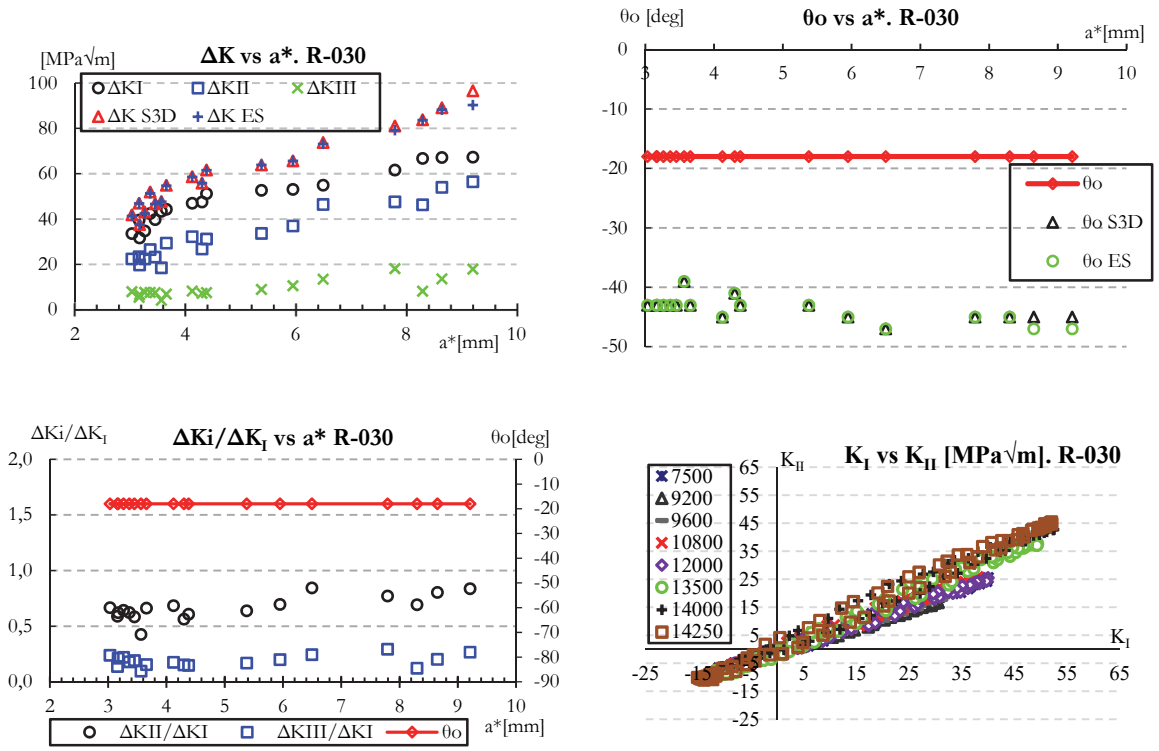


Figure 6: Crack tip parameters measured and calculated for specimen R-030, proportional tension and torsion loads.

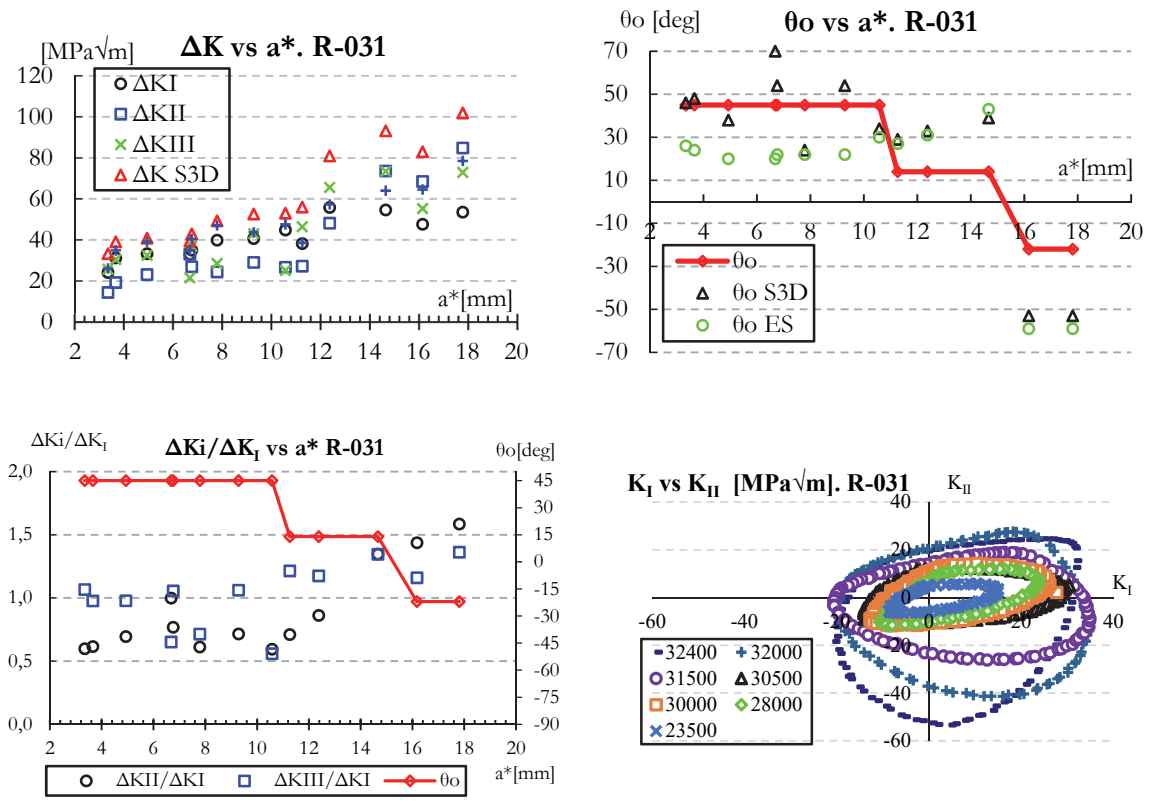


Figure 7: Crack tip parameters measured and calculated for specimen R-031, phase shift 90° between tension 33kN and torsion 382Nm loads.

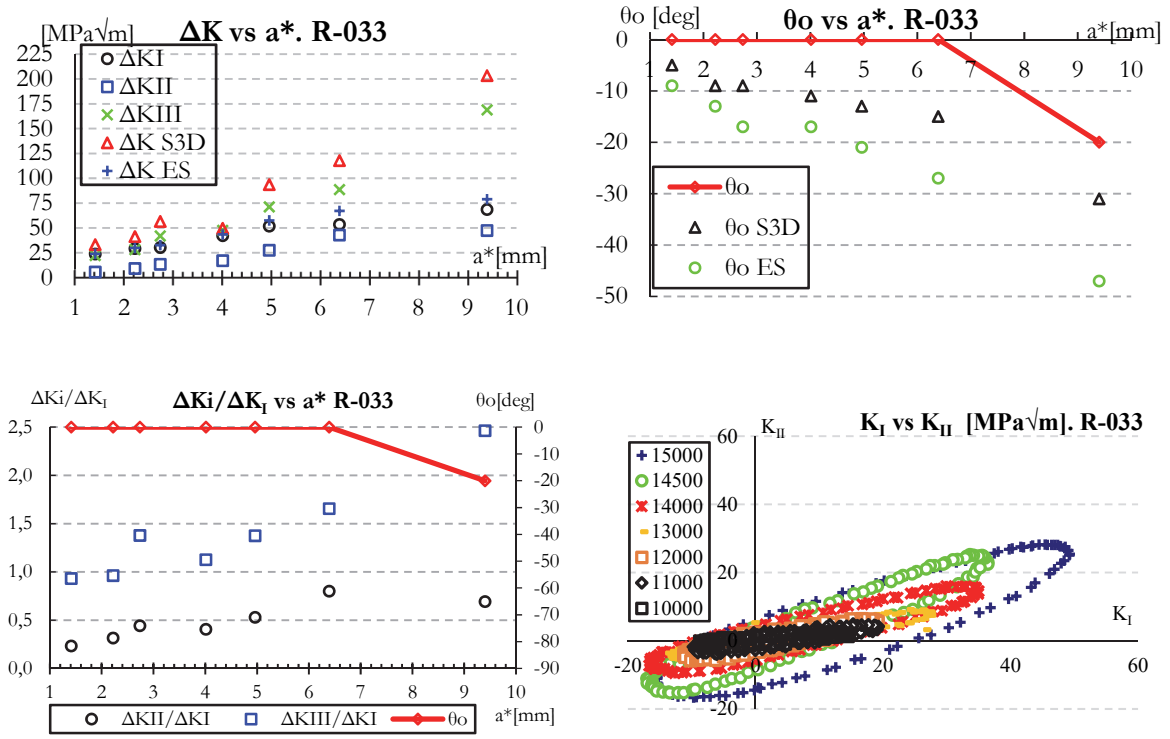


Figure 8: Crack tip parameters measured and calculated for specimen R-033, phase shift 45° between tension 33kN and torsion 382Nm loads.

The second simulation was done with the R-031 specimen (axial and torsional non-proportional mixed load). The crack path was modeled by defining a surface where two parts of the geometry-model are connected. The surfaces (future crack faces) were initially connected with normal surface-to-surface contact, whose properties were changed when a contact surface was being opened. No penetration was allowed in the normal direction and friction was neglected between the crack surfaces. The growth of the crack was achieved by switching these tie constraints along the crack surface to normal contact properties. Due to the complicated geometry of the 3D crack surfaces, linear tetrahedral elements were used to mesh the model. In the simulation, crack growth steps of 1 mm were applied. This step size is not actually recommended. However, achieving convergence was a bigger challenge in this simulation and this large step size was mandatory to achieve any result at all. After several iterations, convergence was achieved up to a crack size of 5 mm. It was not possible to attain convergence after this point, due to the many sources of nonlinearity such as the contact conditions and the complex plasticity model, see [14] for details. Note that, this simulation includes plasticity induced crack closure. The crack closure from the simulation and the experiment for a crack length of 4 mm is given in Fig. 9. In the experiments, the criterion for crack closure was whether the COD was negative or positive. In the simulations, the contact at one of the nodes on the crack surface was considered to be enough for the crack to be closed. The observed crack opening and closing times differ slightly between the simulation and the experiments. Therefore, it can be concluded that the crack closure ranges from simulations can be seen as an acceptable source of information regarding crack closure ranges. More simulations have to be done in the future with other phase angles, or other types of non-proportional loadings to derive an overall conclusion. However, this comparison can be seen as promising and is expected to be a good foundation for future studies.

A second result from the simulations was the crack tip parameters calculated from these simulations. As indicated before, the effective cyclic $\Delta J_{eff}$-integral was used as a crack tip parameter. For the crack lengths of 3mm and 4mm and the given loading pattern nearly identical values of $\Delta J_{eff} \approx 5$ N/mm were obtained. Transformed to an equivalent, plasticity-corrected stress intensity factor gives $\Delta K_{J,eff} \approx 32$ MPa√m. This value can be compared to the corresponding values derived from the DIC-investigation and by applying Eq. (5), Fig. 7. Although the DIC-based values are in the order of magnitude, they appear to be larger, possibly due to the capturing of the mode III contribution. Comparing fatigue crack growth rates for pure mode I (R-028) and non-proportional mixed mode (R-031) it can be concluded that a valid mixed mode hypothesis

should provide a $\Delta K_{eqv,eff} \approx 45$ MPa$\sqrt{m}$ for the case under consideration. It seems that the COD-based hypothesis, Eq. (5), currently is better able to uniquely describe fatigue crack growth under non-proportional mixed mode. Moreover, it provides a growth direction which the energy release rate based approach is currently still lacking.

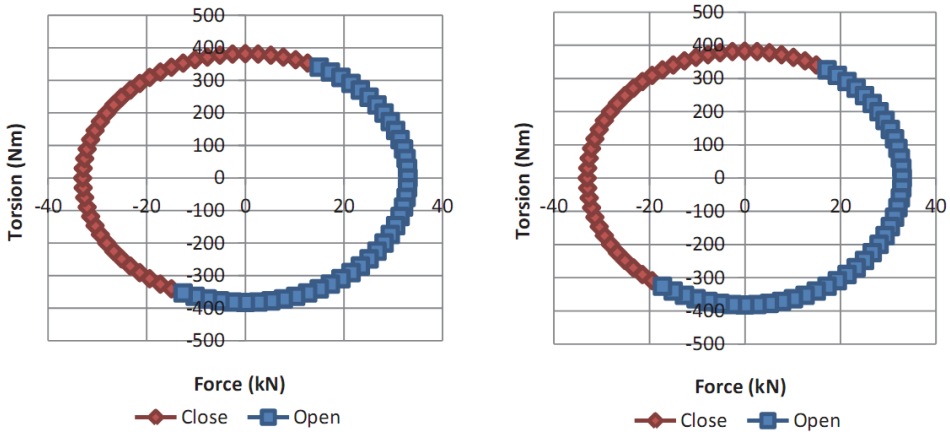


Figure 9: Force-Moment Diagram from the simulation (left) and from experiment (right) of R-031 (axial and torsional non-proportional mixed load), a=4 mm.

## Conclusion

This paper presented a consistent way to determine opening mode SIFs I, II and II from relative crack flank displacements that were measured using the 3D DIC technique. Use of a 3D technique is important because the 2D DIC technique is only applicable to plane problems where out-of-plane displacements are negligible in order not to jeopardize the in-plane measurements. Moreover, the use of 3D DIC allows the measurement of out-of-plane and consequently determinations of mode III crack openings and associated $K_{III}$ values. Calculations of mode III SIF values were useful to show that, in some cases, as for example in the present paper, they may be higher than the mode I and II SIFs and therefore influence the calculation of equivalent static SIFs and cyclic SIF ranges. This paper also presented a way to calculate equivalent SIF ranges for non-proportional loading problems using formulations already presented in literature for proportional loading. In addition, crack tangent directions were calculated from the angles where the maximum equivalent SIF range was found.
Finally, it was shown that mix-mode I, II and III were present in four of the tested specimens, and that the ratio between SIFs II and I varied considerably during one cycle and from cycle to cycle for the non-proportional loaded specimens.

## Acknowledgement

The German Research Foundation (Deutsche Forschungsgemeinschaft) is greatly acknowledged by the authors for financial support under grant Vo729/13-1.

## References

[1] Mróz, K.P., Mróz, Z., On crack evolution rules, Engineering Fracture Mechanics, 77 (2010) 1781-1807.
[2] Zerres, P., Vormwald, M., Review of fatigue crack growth under non-proportional mixed-mode loading, International Journal of Fatigue, 58 (2014) 75–83. DOI: 10.1016/j.engfracmech.2010.02.008.
[3] Schöllmann, M., Richard, H.A., Kullmer, G., Fulland, M., A new criterion for the prediction of crack development in multiaxially loaded structures, International Journal of Fracture, 117 (2002) 129-141. DOI: 10.1023/A:1020980311611.

[4] Richard, H.A., Schramm, B., Schirmeisen, N.-H., Cracks on mixed mode loading – Theories, experiments, simulations, International Journal of Fatigue, 62 (2014) 93-103. DOI: 10.1016/j.ijfatigue.2013.06.019.
[5] Richard, H.A., Fulland, M., Sander, M., Theoretical crack path prediction, Fatigue Fract Engng Mater Struct, 28 (2005) 3-12. DOI: 0.1016/j.ijfatigue.2013.06.019.
[6] Richard, H.A., Eberlein, A. Material Characteristics at 3D-mixed-mode-loadings, Procedia Structural Integrity, 2 (2016) 1821-1828. DOI: 10.1016/j.prostr.2016.06.229.
[7] Y. Yang, M. Vormwald, Three-dimensional fatigue crack growth path simulation under non-proportional mixed-mode loading, 13th International Conference on Fracture, June 16-21, 2013, Beijing, China.
[8] Z. He, A. Kotousov, On the Evaluation of Stress Intensity Factor from In-Plane and Transvers Surface Displacements, Experimental Mechanics, 56 (2016) 1385-1393. DOI: 10.1007/s11340-016-0176-8.
[9] Erdogan, F., Sih, C.G., On the crack extension in plates under plane loading and transvers shear , J. Basic Eng., 1963, 8, 519-525. DOI: 10.1115/1.3656897.
[10] Y. Hos, M. Vormwald, J.L.F. Freire, Measurement and simulation of strain fields around crack tips under mixed-mode fatigue loading, Frattura ed Integrità Strutturale, 33 (2015) 42-55. DOI: 10.3221/IGF-ESIS.33.06.
[11] Y. Hos, J.L.F. Freire, M. Vormwald, Measurements of Strain Fields around Crack Tips under Proportional and Non-Proportional Mixed-Mode Fatigue Loading, International Journal of Fatigue, 89 (2016) 87-98. DOI: 10.1016/j.ijfatigue.2016.01.018.
[12] Gonzáles, G. L. G., Diaz, J. G., González, J. A. O., Castro, J. T. P., & Freire, J. L. F., Determining SIFs Using DIC Considering Crack Closure and Blunting. In Experimental and Applied Mechanics, 4 (2017) 25-36. Springer International Publishing. DOI: 10.1007/978-3-319-42028-8_4.
[13] Nowell, D., Kartal, M.E., de Matos, P.F.P., Digital image correlation measurements of near-tip fatigue crack displacement fields: constant amplitude loading and load history effects, Fatigue and Fracture of Engineering Materials and Structures, 36 (2012) 3-13. DOI: 10.1016/j.ijfatigue.2008.12.003.
[14] Hos, Y., Vormwald, M., Experimental study of crack growth under non-proportional loading along with first modeling attempts, International Journal of Fatigue, 92 (2016) 426-433. DOI: 10.1016/j.ijfatigue.2016.03.036.